Supplementary Information

Gold-silver alloy semi-nanoshell arrays for label-free plasmonic biosensors

Valentina Russo,[a] Niccolo' Michieli,[a] Tiziana Cesca,*[a] Carlo Scian,[a] Davide Silvestri,[b] Margherita Morpurgo,[b] and Giovanni Mattei *[a]

[a] University of Padova, Department of Physics and Astronomy, NanoStructures Group, via Marzolo 8, I-35131 Padova, Italy. E-mail: tiziana.cesca@unipd.it, giovanni.mattei@unipd.it

[b] Department of Pharmaceutical and Pharmacological Sciences, University of Padova, via Marzolo 5, I-5131 Padova, Italy

S1 – FEM Simulations

We report the results of FEM simulations carried out to determine the best-performing metal to be used in the fabrication of SNSA (pure gold or gold-silver alloy) and to investigate the role of the shell roughness in the samples. In these studies, we focused on the bulk sensitivity of the SNSA sensors. The SNSA have been geometrically modeled according to the morphological data collected by SEM and AFM. The dielectric functions are those measured on flat films, as already reported in the main manuscript.

S1.1 – Simulations details

FEM Simulations were performed on the hexagonal lattice unit cell. The unit cell contains one semi-nanoshell (SNS). Also the residual metal on the substrate was modeled, as a nanohole array with the hole placed directly under the shell. The boundaries orthogonal to the substrate plane were modeled by putting periodic boundary conditions. In the $\hat{z}$ direction, orthogonal to the substrate plane, the media over and under the shells array were modeled as semi-infinite using Perfectly Matched Layers (PML). The SNS monomer geometry was modeled, according to the images taken by SEM, as follows. The core was modeled as the union of two oblate semi-ellipsoids having the same XY semi-axes R_{in}, and different Z semi-axes, h_{in}^{+} for the upper part and h_{in}^{-} for the lower part. The external surface of the shell was defined as the union of two ellipsoids, once again with the same XY semi-axes R_{out} and Z semi-axes h_{out}^{+} and $h_{out}^{-} = h_{in}^{-}$. The metal region (shell) was the one bounded by these two surfaces. The shell was truncated and rounded (with a curvature radius of 10 nm) at a distance d_s from the substrate plane. The values for the previous parameters were measured using SEM images for the different configurations considered. The dielectric functions of the materials were taken from ellipsometric measurements performed on optically thick films deposited on a silicon substrate under the same conditions of the SNSA. The radiation wavevector was directed along the $\hat{z}$ axis, downwards. The polarization of the electric field E was along the $\hat{x}$ -axis. The commercial software COMSOL Multiphysics 5.1 was used to solve the Helmholtz equation in the frequency domain for the depicted structure, orthogonally illuminated by plane waves.

S1.2 – Comparison between Au and AuAg alloy SNSA sensors

Fig. S.1 shows the comparison between the simulated absorbance spectra of a pure Au and a AuAg SNSA sensor (HI configuration), for n=1.0 and n=1.5.

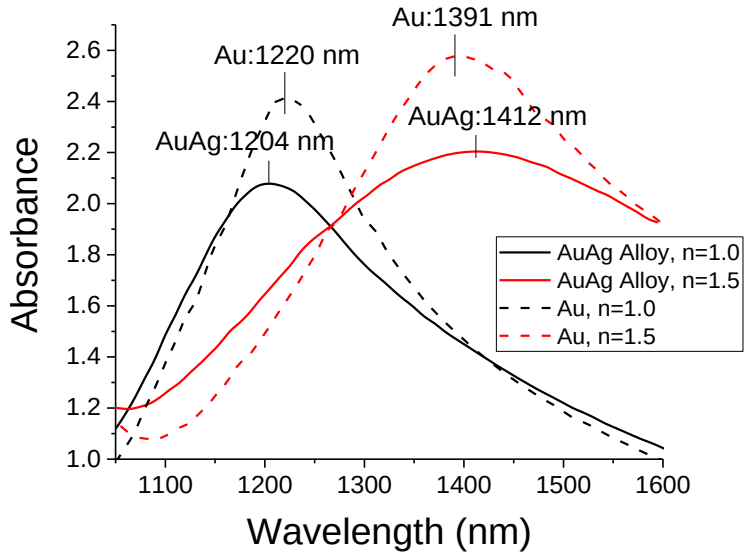

S.1 – Simulated absorbance spectra computed for a pure Au (solid lines) and a AuAg alloy (dashed line) SNSA, in two different dielectric environments. Black lines correspond to SNSA embedded in air (n=1.0), red lines correspond to SNSA embedded in a medium with refractive index n=1.5.

From these spectra, the bulk sensitivity is computed using the formula:

$$S_{bulk} = \frac{\Delta\lambda}{\Delta n}.$$

The bulk sensitivity of the AuAg alloy SNSA results: $S_{bulk}^{AuAg} = 416 \pm 10\, nm/RIU$, whereas for the Au SNSA we get: $S_{bulk}^{Au} = 342 \pm 10\, nm/RIU$. The sensitivity of AuAg SNSA is more than 20% higher than that of Au SNSA. Thus, AuAg alloy was chosen for the fabrication of the samples.

S1.3 – Study of the role of roughness

We performed a study on the role of the shell roughness on the shape and position of the resonances, and on the bulk sensitivity of the sensors, comparing the results of FEM simulations of a SNSA sensor with flat semi-nanoshell surface and a rough one. A random roughness with an amplitude of about 20 nm was introduced in the model. Fig. S.2 shows the comparison between the simulated absorbance spectra obtained in the two cases, for n=1.0 and for n=1.5.

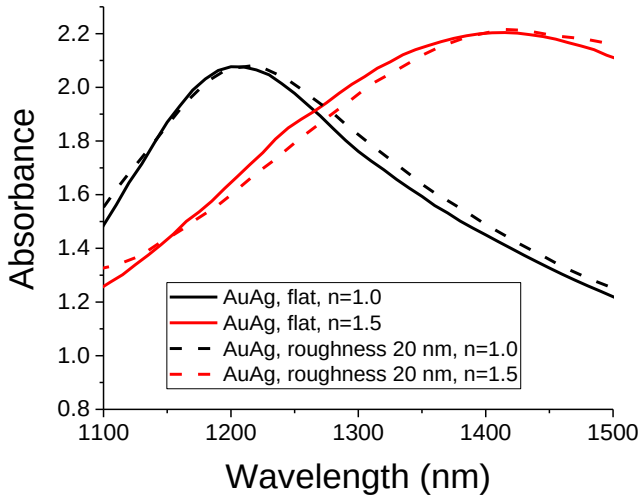

S.2 – Simulated absorbance spectra computed for AuAg alloy SNSA, with and without roughness, in two different dielectric environments. Solid lines indicate the spectra computed for a flat SNSA, dashed lines for a SNSA with a 20 nm amplitude random roughness. Black lines correspond to SNSA embedded in air (n=1.0), red lines correspond to SNSA embedded in a medium with refractive index n=1.5.

The graph shows that in both cases the presence of a shell roughness gives rise to a modest shift of the resonance (less than 10 nm), definitely much smaller than the width of the resonances themselves. Thus, the effect of roughness can be considered to be convoluted inside the global broadening of the resonances due to defects. Moreover, as the resonance shifts are small, also the bulk sensitivity results almost unaffected by the presence of the roughness, and the differences are less than 1%. This is due to the fact that, particularly for high-interaction (HI) semi-nanoshells, field confinement and enhancement are mainly affected by the interaction between nearby semi-nanoshells and not merely by the metal/dielectric interface. Thus, the fine morphology of the metallic shells is not so crucial in the formation of resonances.

S2 – Bulk Sensitivity measurements

S2.1 – Semi-nanoshell array (SNSA)

Here we present the bulk sensitivity measurements performed on SNSA in the HI configuration. Experimental absorbance spectra were measured in air and using NOA-61, from Corning (n=1.542), as the high refractive index medium. Water is not suitable for measurements in the IR wavelength range since its characteristic absorption bands overlap the resonance peaks.

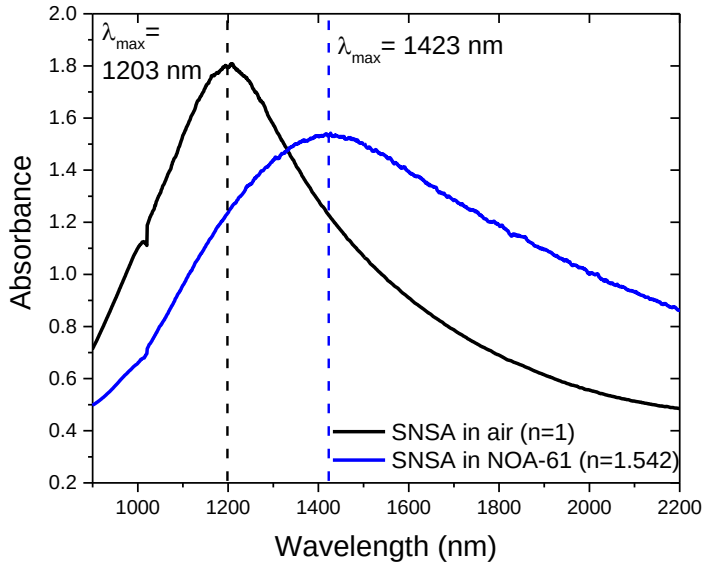

S.3 – Experimental absorbance spectra of the AuAg HI-SNSA embedded in air (n=1.0, black line) and in NOA-61 (n=1.542, blue line).

The resulting sensitivity is in this case $S_{bulk}^{exp} = 405 \pm 10\, nm/RIU$. This result is in good agreement with the simulations presented in section S1, from which a bulk sensitivity of $S_{bulk}^{FEM} = 416 \pm 10\, nm/RIU$ was obtained.

S2.2 – Ag Nanoprism Array (NPA)

In this section we present the experimental absorbance spectra of a Ag NPA measured in air (n=1) and in water (n=1.33). In this case, the bulk sensitivity results $S_{bulk}^{exp} = 250 \pm 10\, nm/RIU$, in agreement with previously reported simulations $S_{bulk}^{FEM} = 240 \pm 10\, nm/RIU$ (see Ref. 39 of the main manuscript).

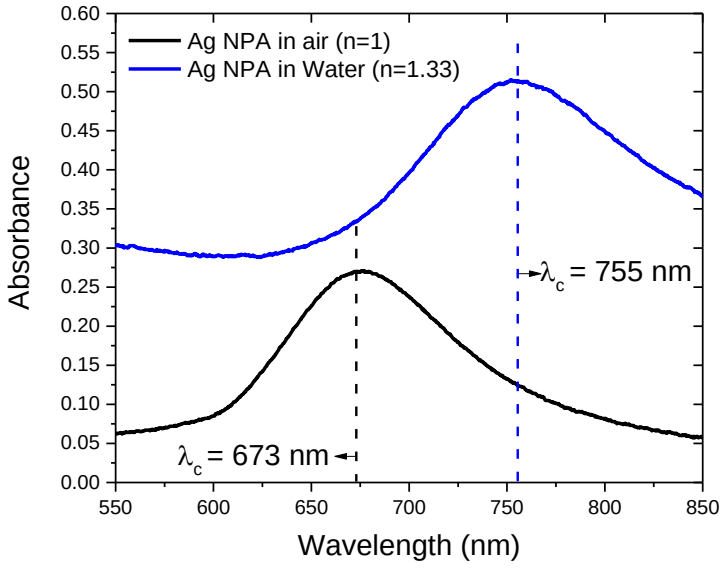

S.4 – Experimental absorbance spectra of a Ag NPA embedded in air (black line) and in water (blue line).

S3 – AuAg optical constants

The optical constants measured by ellipsometry of AuAg films deposited by magnetron sputtering, before and after annealing at 300 °C degrees in air are reported in Fig. S5.

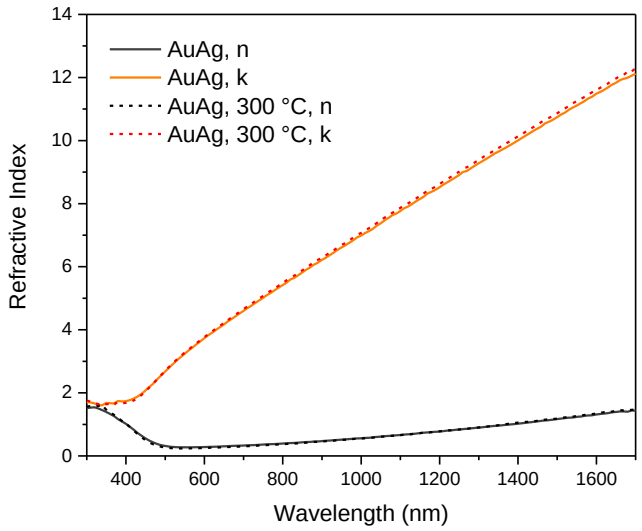

S.5 – Experimental optical constants measured by ellipsometry of AuAg films deposited by magnetron sputtering, before (solid lines) and after (dashed lines) annealing at 300 °C in air.